Journal of Catalysis 351 (2017) 1–9

Contents lists available at ScienceDirect

Journal of Catalysis

journal homepage: www.elsevier.com/locate/jcat

Photocatalytic water-splitting solar-to-hydrogen energy conversion: Novel $LiMoO_3(IO_3)$ molybdenyl iodate based on WO_3-type sheets

Ali H. Reshak [a,b,*], Sushil Auluck [c,d]

[a] New Technologies – Research Centre, University of West Bohemia, Univerzitni 8, 306 14 Pilsen, Czech Republic
[b] School of Material Engineering, University Malaysia Perlis, 01007 Kangar, Perlis, Malaysia
[c] Council of Scientific and Industrial Research – National Physical Laboratory Dr. K S Krishnan Marg, New Delhi 110012, India
[d] Department of Physics, Indian Institute of Technology, Hauz Khas, New Delhi 110016, India

ARTICLE INFO

Article history:
Received 12 March 2017
Revised 26 March 2017
Accepted 28 March 2017

Keywords:
Electronic structure
Molybdenyl iodate
Electronic charge density distribution
Photocatalysts

ABSTRACT

The electronic structure of the novel molybdenyl iodate $LiMoO_3(IO_3)$ based on WO_3-type sheets is calculated in order to understand to its usage as a photocatalyst. Using X-ray diffraction data as the initial input, we have optimized the atomic positions by minimizing the force on each atom. Calculations are performed using the generalized gradient approximation (PBE-GGA) within the full-potential linear augmented plane wave method. The optimized structure is used to calculate the electronic band structure and the related properties with PBE-GGA and the recently modified Becke–Johnson potential (mBJ). The top of the valence band (VBM) and the bottom of the conduction band (CBM) are located at the Γ point of the Brillouin zone (BZ), resulting in a direct energy band gap of 2.15 eV (PBE-GGA) or 2.73 eV (mBJ). It is clear that mBJ succeeds by a large amount in bringing the calculated energy gap into close agreement with the measured one (2.80 eV). Thus, $LiMoO_3(IO_3)$ could be an active visible-light photocatalyst. The angular-momentum-resolved projected density of states reveals that the energy gap value is mainly controlled by O2*p* (valence bands) and Mo4*d* (conduction bands) states. The electronic charge density distribution is calculated in two crystallographic planes to explore the chemical bonding characters. The free end Li atom forms ionic bonds, whereas the I atom forms partial valence and dominant ionic bonds with two O atoms. Mo and Li atoms form very weak covalent bonds with O atoms. The calculated chemical bond lengths and angles are in good agreement with the experimental values.

1. Introduction

Solar energy is the most promising form nonpolluting renewable energy [1–4]. To utilize solar energy, numerous investigations on efficient photocatalytic materials have been performed with a view to finding alternative clean energy resources [5–7]. The semiconductors that absorb light and generate photoexcited electrons and holes to participate in redox reactions are the most efficient photocatalyst materials [8–10]. It has been reported that the semiconductors with wide energy band gaps possess higher redox ability [11]. To enable photocatalyst activity in visible light a band gap in the range of 1.5–3.0 eV is needed.

In the last two decades, several molybdenyl iodates have been identified as novel and interesting materials in photonic technology, nonlinear optics, and laser engineering [12–19]. Moreover, several iodate photocatalysts with high photocatalytic activity have recently been reported [20–25]. The visible light absorption may be derived from the band transition between O2*p* and Mo4*d*, which leads to production of high-density hot charge carriers, resulting in increasing the photocatalytic activity [20]. Therefore, based on previous works on the iodate photocatalysts [21–25], we have addressed ourselves to investigating the ground state properties of the novel molybdenyl iodate $LiMoO_3(IO_3)$ in order to understand its usage as a photocatalyst.

There have been numerous efforts to develop new photocatalysts. The present study is aimed to provide an understanding of developing high-performance photocatalysts. Huang et al. [25] have investigated the photocatalytic activity of $BiIO_4$ and $Bi(IO_3)_3$, two novel Bi-based iodates. They have reported that, similarly to the Bi^{3+} cation, the IO_3^- anion also contains lone pair electrons. These lone pair electrons very strongly favor the formation of layered structures of crystals. Huang et al. investigated the photocatalytic performance of $BiIO_4$ and $Bi(IO_3)_3$ with layered structures and found that they exhibit excellent photocatalytic activity.

* Corresponding author at: New Technologies – Research Centre, University of West Bohemia, Univerzitni 8, 306 14 Pilsen, Czech Republic.
E-mail address: maalidph@yahoo.co.uk (A.H. Reshak).

http://dx.doi.org/10.1016/j.jcat.2017.03.020
0021-9517/

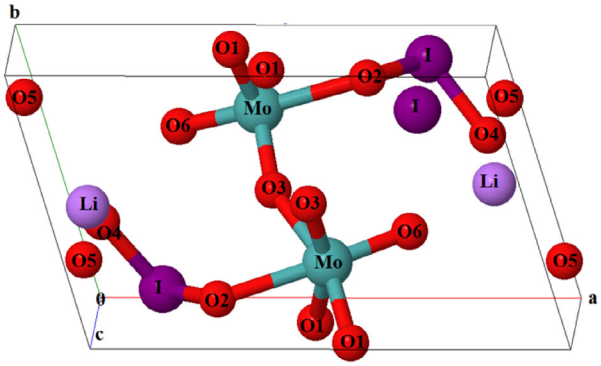

(a) The unit cell of $LiMoO_3(IO_3)$ contains two formula which counted as a typical representation of the combination of distorted MoO_6 octahedron and IO_3^- group

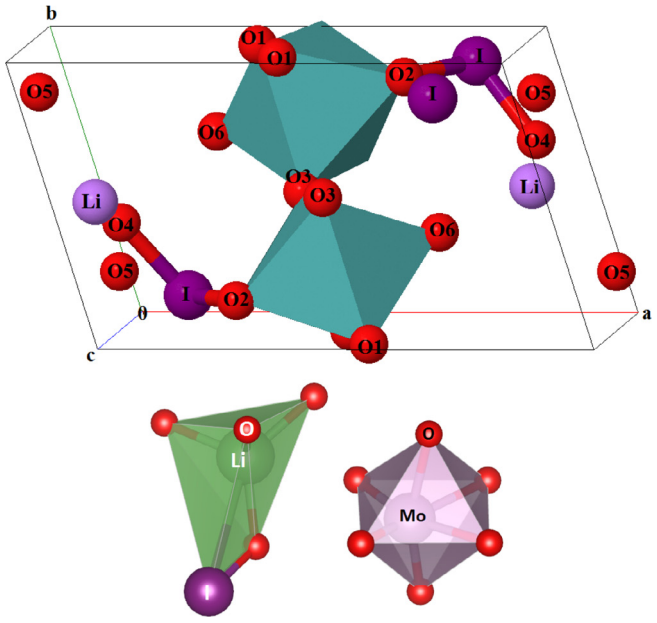

(b) distorted MoO_6 octahedron and IO_3^- group

Fig. 1. (a) The relaxed structure of $LiMoO_3(IO)_3$. The unit cell of $LiMoO_3(IO)_3$ contains two formulae that count as a typical representation of the combination of a distorted MoO_6 octahedron and an IO_3^- group. (b) A distorted MoO_6 octahedron and an IO_3^- group.

Table 1
The optimized atomic positions obtained by PBE-GGA in comparison with the experimental data [12].

	x-Exp.	*x*-Opt.	*y*-Exp.	*y*-Opt.	*z*-Exp.	*z*-opt.
I	0.37670(9)	0.37777	0.38418(9)	0.37998	0.33664(5)	0.32988
Mo	0.23487(11)	0.22989	0.61524(12)	0.60988	−0.03549(7)	0.97862
O1	0.4908(12)	0.50001	0.8199(13)	0.82346	−0.0428(8)	0.94568
O2	0.3574(13)	0.34587	0.6601(12)	0.65987	0.2140(7)	0.22123
O3	−0.0183(12)	0.9715	0.8332(12)	0.82234	−0.0432(8)	0.94542
O4	0.1196(14)	0.12134	0.4619(13)	0.45999	0.4168(8)	0.41778
O5	0.6504(13)	0.64321	0.4872(15)	0.49121	0.4898(8)	0.49887
O6	0.1426(13)	0.13989	0.4884(13)	0.47989	−0.2200(8)	0.77111
Li	−0.006(4)	0.9899	0.806(4)	0.81121	0.417(3)	0.41459

The combination of d^0 transition metals and stereoactive lone pairs containing cations seems to be a very promising combination for creating polar materials with pronounced optical properties [26]. This combination is susceptible to second–order Jahn–Teller (SOJT) distortion [27,28]. One good example of this is the alkali metal Mo(VI)–iodate compounds, which are a typical combination of a distorted MoO_6 octahedron and an IO_3^- group [12,13]. Chen et al. [12] have obtained $LiMoO_3(IO)_3$ as a new member of these compounds, which crystallizes in the polar and chiral space group $P2_1$. They reported that the newly discovered $LiMoO_3(IO)_3$ has an unprecedented layered structure consisting of WO_3^- -type sheets capped by IO_3^- groups.

It is interesting to mention that $LiMoO_3(IO)_3$ has a novel structure. It is a layered material containing $[MoO_3(IO_3)]^{1-}$ anionic lay-

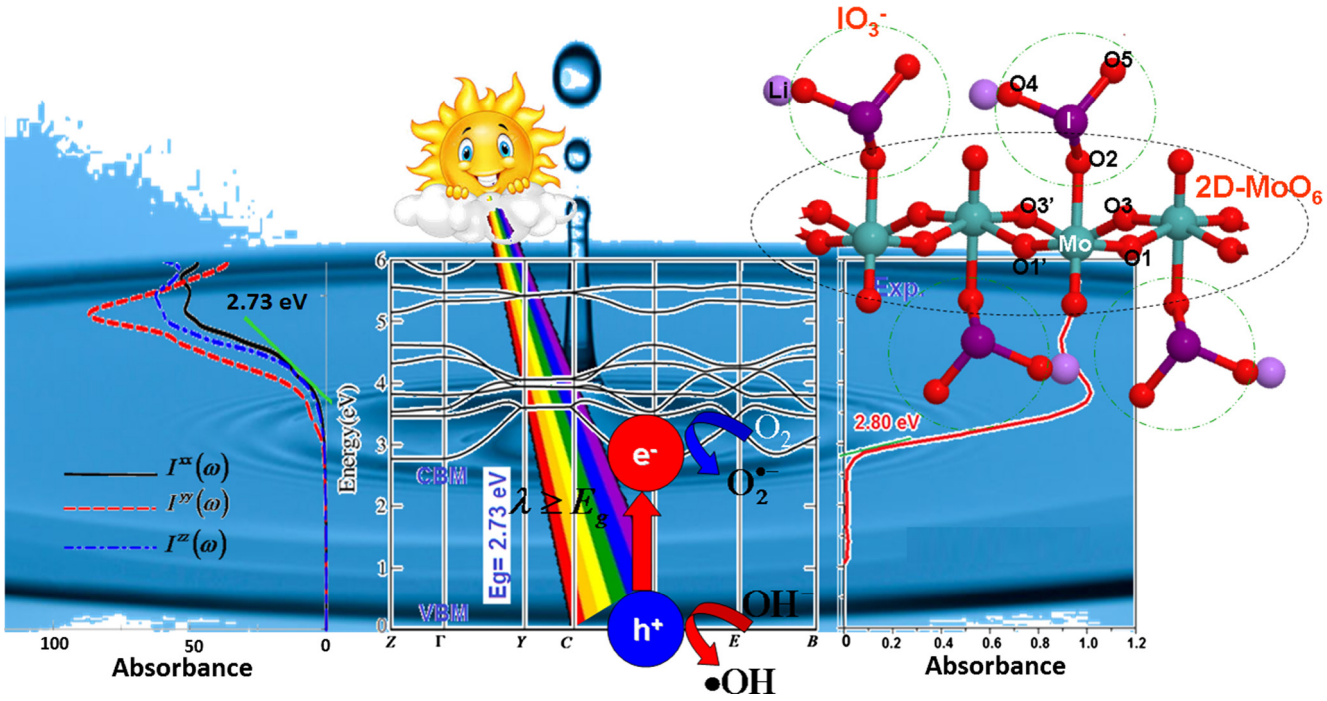

Fig. 2. Schematic diagrams of charge transfer and photocatalytic mechanism of $LiMoO_3(IO_3)$. (Left panel) calculated absorbance of $LiMoO_3(IO_3)$; (intermediate panel) electronic band structure of $LiMoO_3(IO_3)$; (right panel) to reproduce the data of the measured optical absorption spectra of $LiMoO_3(IO_3)$, we have used special software to extract the experimental data from the figure provided in Ref. [12]; then we replotted the extracted data and compared them with the electronic band structure. When the photocatalyst absorbs radiation from sunlight, it will produce pairs of electrons and holes. The electron of the valence band becomes excited when illuminated by light. The excess energy of this excited electron promotes it to the conduction band, creating a negative electron (e^-) and positive hole (h^+) pair. This is referred as the semiconductor's photoexcitation state.

ers separated by Li^+ counterions [12]. We should emphasize that the oxide nanoparticles should make a substantial contribution to optical effects due to the high contribution of the phonon subsystem to the trapping levels [29,30]. It is well known that the layered configuration induces internal static electric fields and polar IO_3^- groups, resulting in polarized electric fields that are beneficial to the separation of photogenerated charge carriers [22]. Previous theoretical work on $LiMoO_3(IO)_3$ [19] has been carried out using a non-full-potential method within the generalized gradient approximation (PBE-GGA) [31], which may cause some uncertainty due to ignoring the potential in the interstitial region and also due to the well-known underestimation of the energy band gap caused by using PBE-GGA. As the value of the energy band gap is a very important factor in photocatalysts, we decided to perform a comprehensive theoretical calculation based on a full-potential method to ascertain the influence of the full potential on the electronic structure and, hence, the energy band gap, which has a crucial influence on the resulting properties of $LiMoO_3(IO)_3$. To overcome the drawback of PBE-GGA, we have used the recently modified Becke–Johnson potential (mBJ) [32] to bring the calculated energy gap into close agreement with the experimental value. Based on our experiences with mBJ, we would like to mention here that in our previous work [33–37] we have calculated the energy band gap using mBJ on several systems whose energy gaps were known experimentally. In these calculations, we found very good agreement with the experimental data. Thus, we believe that our calculations reported in this paper will produce very accurate and reliable results. In recent years, due to improvement in computational technologies, it has been proven that first-principles calculation is a strong and useful tool to predict the crystal structure and properties related to the electronic configuration of a material before its synthesis [29,38–41]. Several researchers have used first-principles calculation to explore new photocatalysts [42–45].

2. Calculation methodology

The calculations are performed using the X-ray crystallographic data for $LiMoO_3(IO)_3$ reported by Chen's group [12]. The positions of atoms were relaxed to minimize the forces on the atoms (1 mRy/A). We have used the generalized gradient approximation (PBE-GGA) [31] within the full-potential linear augmented plane wave (FPLAPW + lo) method as embodied in the WIEN2k code [46]. The resulting relaxed geometry was used to calculate the electronic structure and the associated electronic properties using PBE-GGA and the recently modified Becke–Johnson potential (mBJ) [32]. The relaxed crystal structures of $LiMoO_3(IO)_3$, along with the unit cell, are presented in Fig. 1. The relaxed geometry is given in Table 1 and is compared with the experimental data [12]. The potential for the construction of basis functions inside the sphere of the muffin tin was spherically symmetric, whereas outside the sphere it was constant [47]. The muffin-tin radii (R_{MT}) of the atoms were chosen in such a way that the spheres did not overlap. The value of R_{MT} is taken to be 1.84 a.u. (I), 1.71 a.u. (Mo), 1.55 a.u. (O), and 1.63 a.u. for Li. To achieve total energy convergence, the basis functions in the interstitial region (IR) were expanded up to $R_{MT} \times K_{max} = 7.0$ and inside the atomic spheres for the wave function. The maximum value of $\boldsymbol{l}$ was taken as $\boldsymbol{l}_{max} = 10$, while the charge density is Fourier expanded up to $G_{max} = 12(a.u.)^{-1}$. Self-consistency is obtained using 300 $\vec{k}$ points in the irreducible Brillouin zone (IBZ). The self-consistent calculations are converged, since the total energy of the system is stable within 0.00001 Ry. The electronic properties

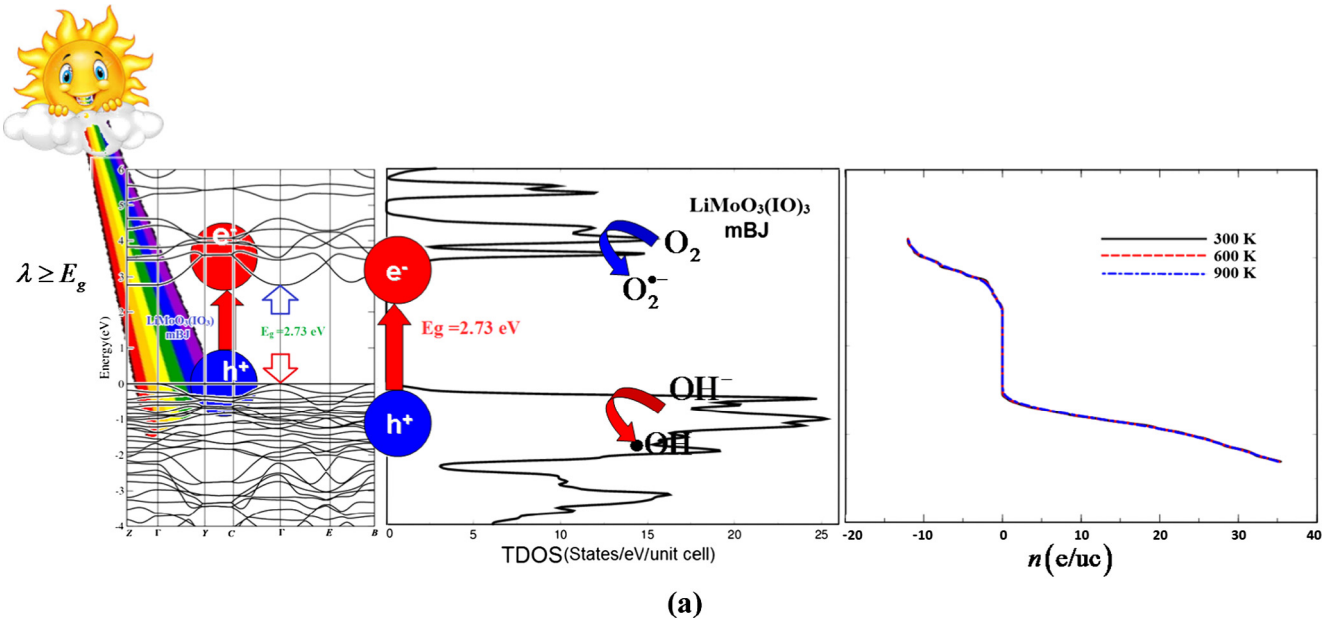

(a)

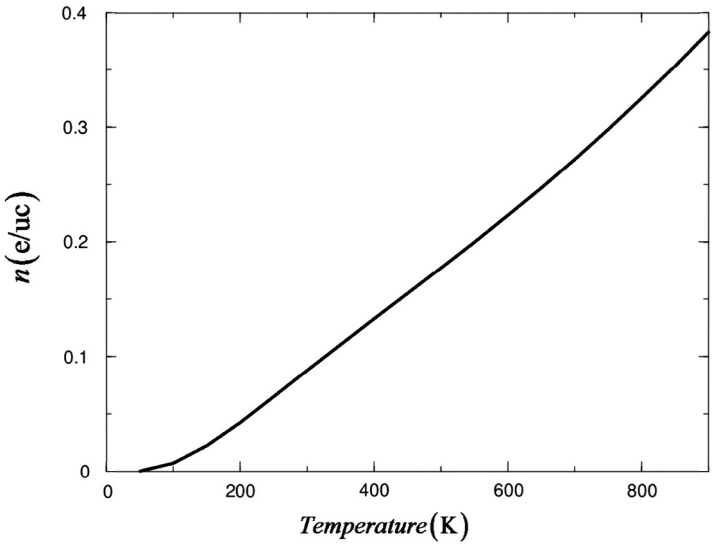

(b)

Fig. 3. (a) (Left panel) calculated electronic band structure of $LiMoO_3(IO)_3$; (intermediate panel) calculated total density of states; (right panel) carrier concentration as function of chemical potential $\mu - E_F$ at three temperatures. (b) Carrier concentration as a function of temperature at fixed chemical potential ($\mu = E_F$). (c–h) Calculated partial densities of states.

are calculated using 1500 $\vec{k}$ points in the IBZ. The total and partial density of states (DOS) were calculated by means of the modified tetrahedron method [48]. The input required for DOS is the energy eigenvalues and eigenfunctions that are the natural outputs of the band structure calculation.

3. Results and discussion

3.1. Electronic band structures and density of states

When a photocatalyst absorbs radiation from sunlight, it produces electron–hole pairs. The valence band electron becomes excited when it absorbs a photon. The excess energy of this excited electron promotes it to the conduction band, creating electron (e−)–hole (h^+) pairs. This stage is referred as the semiconductor's photoexcitation state. To explain this mechanism in $LiMoO_3(IO_3)$, the electronic band structure along with the calculated absorbance and measured one [12] are presented in Fig. 2. It is clearly shown that the calculated fundamental optical absorption edge is located at 2.73 eV (λ = 454.5 nm) and matches the experimental value of the absorption edge (2.80 eV, λ = 443.1 nm). Thus, the $LiMoO_3(IO_3)$ can respond to visible light. The photocatalytic evaluation is carried out by calculating the absorbance spectrum at characteristic bands and comparing it with the measured spectrum [12], as shown in Fig. 2. We would like to mention that to reproduce the data of the measured optical absorption spectra of $LiMoO_3(IO_3)$ in the right panel in Fig. 2, we used special software to extract the experimental data from the figure provided in Ref. [12]. Then we replotted the extracted data and compared them with the electronic band structure.

Furthermore, to gain deep insight into this mechanism in $LiMoO_3(IO_3)$, the carrier concentration as a function of chemical potential ($\mu - E_F$) at three temperatures is shown in Fig. 3a (right

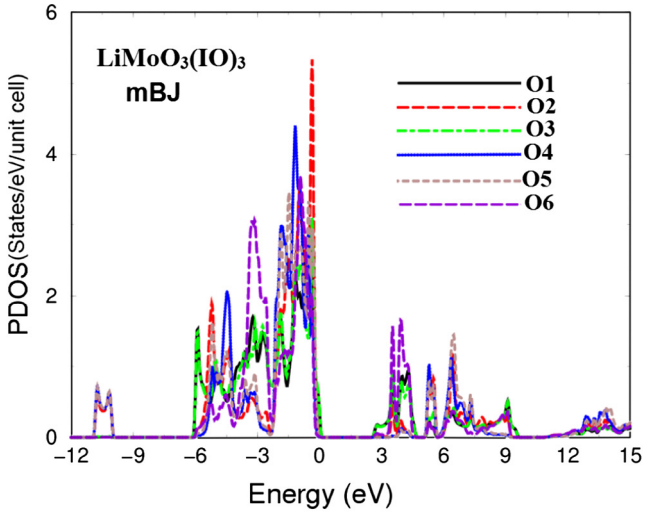

(c)

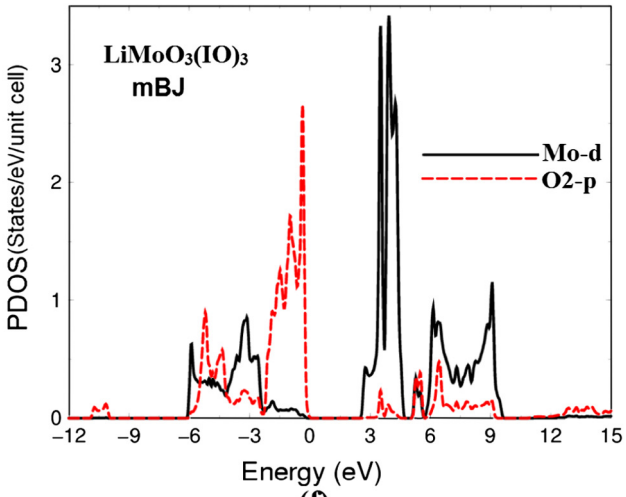

(f)

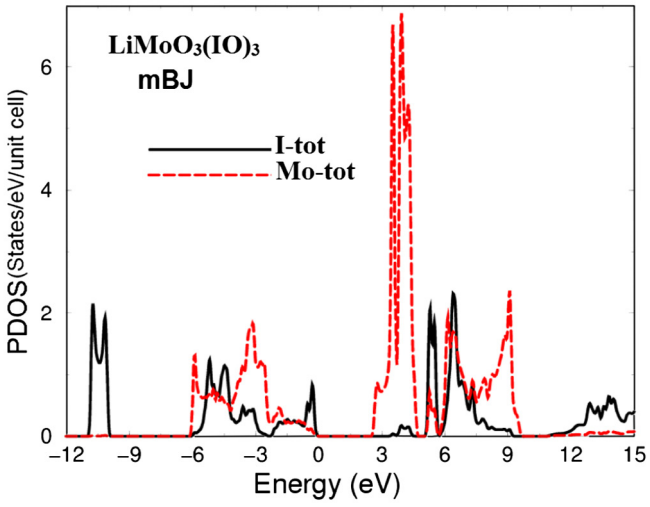

(d)

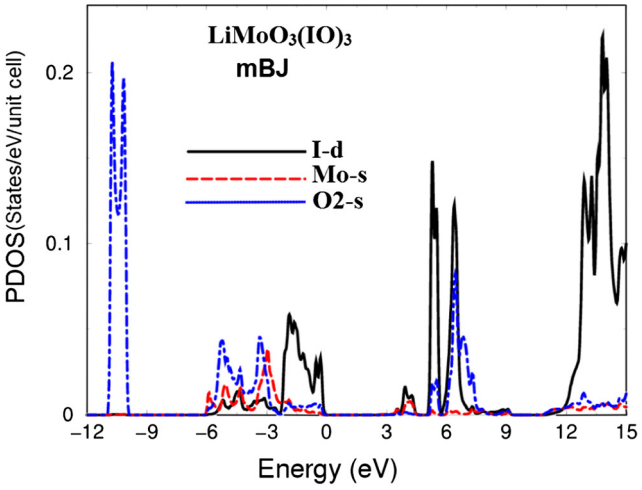

(g)

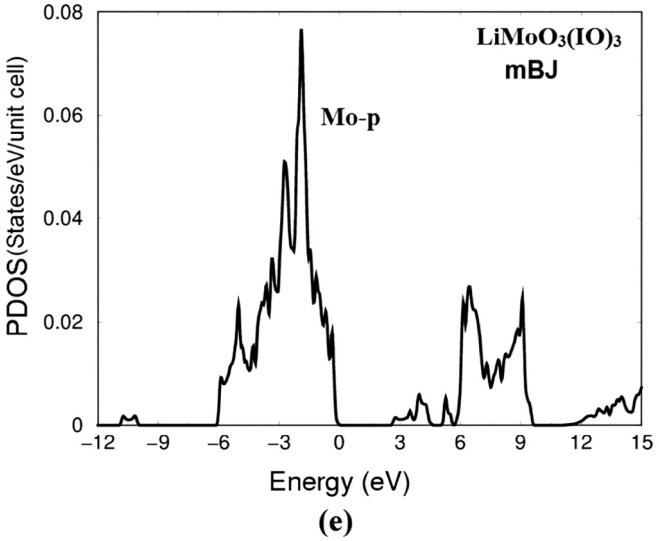

(e)

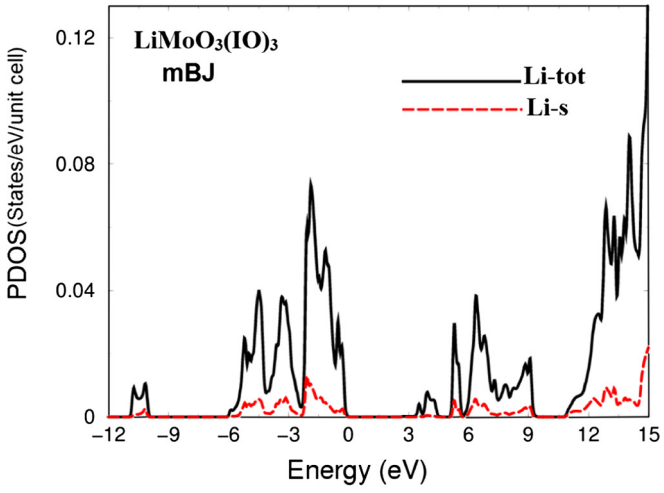

(h)

Fig. 3 (*continued*)

panel). It clearly shows negative electron (n-type conduction) and positive hole (p-type conduction) pairs. The photogenerated electrons of $LiMoO_3(IO_3)$ break apart water molecules to form hydrogen gas and hydroxyl radicals. The negative electrons react with oxygen molecules to form superoxide anions. This cycle continues while light is available. To observe the influence of temperature on the carrier concentration (electrons and holes), the carrier concentration is shown in Fig. 3b as a function of temperature at fixed chemical potential ($\mu = E_F$). It has been noticed that the carrier concentration increases with increasing temperature.

The electronic band structure along the high-symmetry directions of the first BZ and the total density of states (TDOS) are illustrated in Fig. 3a (left panel and intermediate panel). It has been noticed from the electronic band structure that the high k-dispersion bands around the Fermi level (E_F) possess low effective masses and, hence, high-mobility electrons, which enhances the charge transfer process. The top of the valence band (VBM) and the bottom of the conduction band (CBM) are located at the Γ point of the BZ, resulting in a direct energy band gap of about 2.15 eV (PBE-GGA) or 2.73 eV (mBJ). It is clear that mBJ succeeds by a large amount in bringing the calculated energy gap into close agreement with the measured one (2.80 eV) [12] and much better than the previous calculated gap (2.30 eV), which was obtained from the pseudo-potential CASTEP code with PBE-GGA [19]. Therefore, we have decided to show only the results obtained by the mBJ exchange correlation potential. The angular-momentum-resolved projected density of states (PDOS) is presented in Fig. 3c–h. It shows that the VBM is formed by O2*p* states while the CBM by Mo4*d* states. Since the crystal structure of $LiMoO_3(IO)_3$ consists of one Mo atom, one I atom, six O atoms (1–6), and one atom of Li, we show the contribution of each atom in Fig. 3c–h. It is clear that the six O atoms make different contributions to the PDOS. The O2 atom makes the largest contribution. To explore the contribution of each orbital, we have decided to show in Fig. 3c the orbitals of each type of atom, for instance, I – 5s/5p/4d, Mo – 5s/4p/4d, Li – 2s, and the orbitals of O2 – 2s/2p atoms, only because they show large contributions. It has been noticed that there exists a hybridization between O1, O2, O3, O4, and O5 atoms, and that O2 – 2s hybridizes with I – 4d states. The overall hybridization is not strong enough to form pure valence bonding, and, therefore we expected to see strong ionic and partial valence bonds. However, if we compare our calculated PDOS with that obtained by CASTEP-PBE-GGA [19], we find that the PDOS of the I – 4d state is missing. Since I – 4d forms strong hybridization with O2 – 2s and Mo – 5s states, it is necessary to explore it. Moreover, in a previous report, they plot the states of each atom separately without exploring the hybridization between the states of different atoms. The hybridization is essential to analyze the chemical bonding characters, which are very important in understanding the role of each orbital. Therefore, our PDOS plots (Fig. 3c–h) cover the missing information.

The origin of chemical bonding can be elucidated from the angular momentum decomposition of the atoms' projected electronic density of states (PDOS). Integrating the latter from −6.0 eV up to the Fermi level (E_F), we obtain the total number of electrons/eV (e/eV) for the orbitals in each atom of $LiMoO_3(IO)_3$, O1 atom 4.0 e/eV, O2 atom 5.5 e/eV, O3 atom 3.7 e/eV, O4 atom 4.2 e/eV, O5 3.9 e/eV, O6 atom 3.6 e/eV, I atom 1.7 e/eV, Mo atom 1.9 e/eV, and Li atom 0.07 e/eV. The contributions of these atoms to the valence bands show that some electrons from Li, Mo, O, and I atoms are transferred into valence bands and contribute to the covalent interactions between the atoms. The covalent bonds arise due to the hybridization degree and the electronegativity differences between the atoms. According to the Pauling scale, the electronegativities of Li, Mo, O and I are 0.98, 2.16, 3.44, and 2.66. It is clear that there are charge interactions between the atoms due to the existence of the hybridization. Thus, the angular momentum decomposition of the atoms' projected electronic densities of states helps us to analyze the bond nature according to the classical chemical concept. This concept is very useful for classifying compounds into different categories with respect to different chemical and physical properties. The calculated bond lengths (Fig. 4a and b) and angles are listed in Tables 2 and 3 in comparison with the measured ones [12]. It is clear that our calculations are in good agreement with the experimental data, which confirms the accuracy of the calculations, and this is attributed to the use of the full potential with the recently modified Becke–Johnson potential.

3.2. Valence electronic charge density

The valence electronic charge density helps to give a map of the electron distribution and the nature of the chemical bonding between the atoms. Therefore, we have calculated the valence electronic charge density in two crystallographic planes 100 and 101 to explore the anisotropic bonding in the compound. It has been noticed that 100 shows only Li, I, and O atoms. The free end Li atom forms ionic bonding, whereas the I atom forms covalent bonds with two O atoms. The unconnected O atoms are surrounded by uniform spheres, while in the connected O atoms, for instance O–I–O, the interaction causes a perturbation to the uniform spheres, as is clear from Fig. 4c. To illustrate all the atoms and investigate the anisotropy, we have plotted the crystallographic plane in the 101 direction (Fig. 4d), which reveals that Mo and Li atoms form weak covalent bonds with O atoms. The anisotropy between the atoms can be seen from the two crystallographic planes and the calculated bond lengths (Table 2). The strength of the covalent bonds depends on the degree of the hybridizations between the atoms. Due to the electronegativity difference between Li, Mo, O, and I atoms, we can see a charge transfer toward O atoms, as indicated by the blue color around O atoms (according to the thermoscale, the blue color exhibits the maximum charge accumulation).

4. Conclusions

The full-potential method is used for a comprehensive theoretical investigation of the electronic band structure, the angular-momentum-resolved projected density of states, and the electronic charge density distribution of the novel molybdenyl iodate $LiMoO_3(IO_3)$ in order to understand its usage as a photocatalyst. The experimental geometric structure was optimized by minimizing the forces acting on each atom using the PBE-GGA exchange correlation potential. From the resulting geometrical structure, the ground state properties were calculated using the recently modified Becke–Johnson potential (mBJ), which is known to give better energy gaps. The obtained band gap of 2.73 eV is in good agreement with the measured gap of 2.80 eV. The previous calculated gap of 2.30 eV was obtained using the pseudo-potential-based CASTEP code within the generalized gradient approximation (PBE-GGA). This agrees with our PBE-GGA gap of 2.15 eV. Our calculations reveal that the conduction band minimum (CBM) and the valence band maximum (VBM) are located at the center of the Brillouin zone (BZ), resulting in a direct band gap. The angular-momentum-resolved projected density of states explore the orbitals' contributions to the electronic states and the hybridization between the states. It is found that the VBM is formed by O2*p* states and the CBM by Mo4*d* states. The valence electronic charge density was calculated in two crystallographic planes to explore the chemical bonding anisotropy in the investigated compound. The

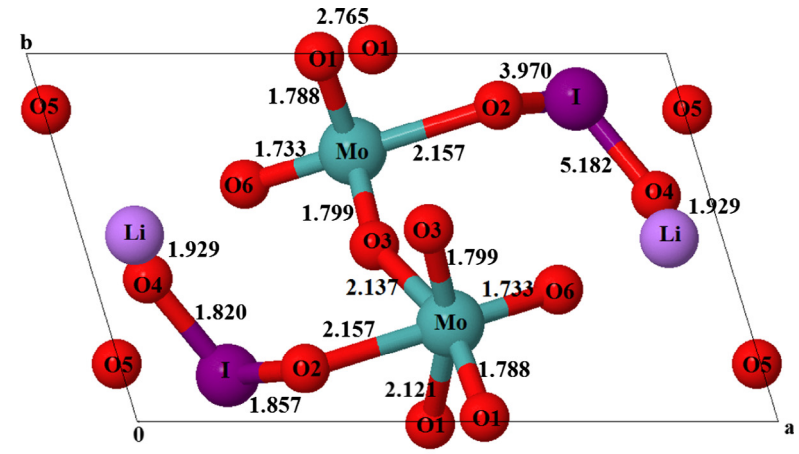

(a)

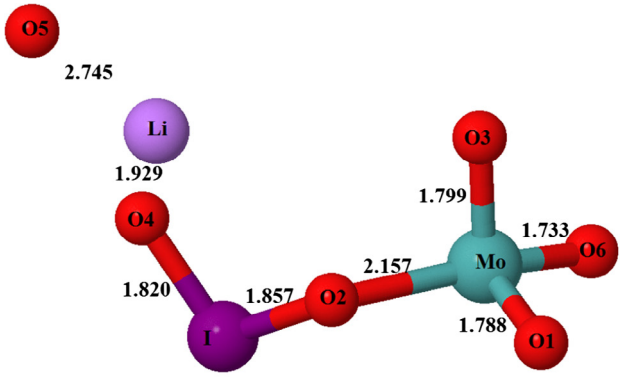

(b)

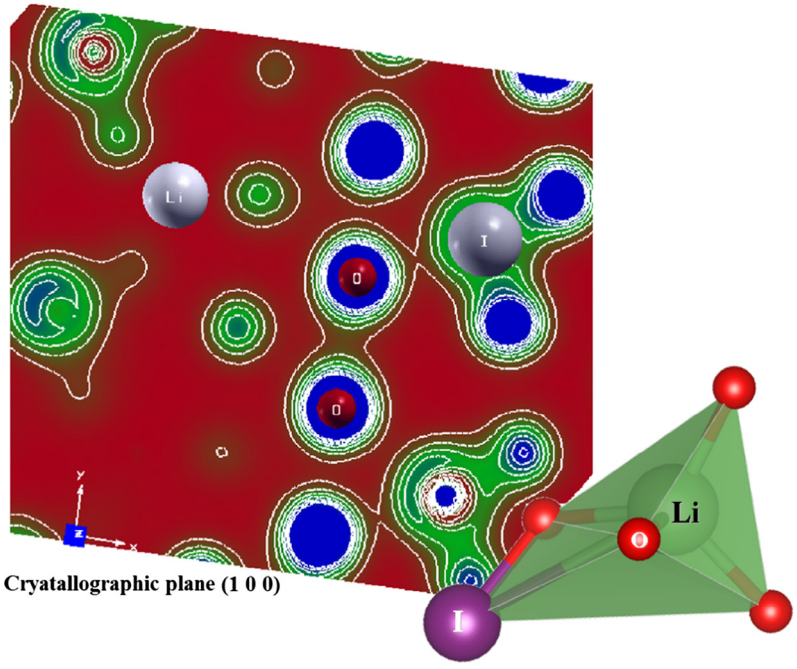

(c)

Fig. 4. (a, b) The calculated bond lengths in the unit cell; (c) the electronic charge density distribution in the (100) crystallographic plane; (d) the electronic charge density distribution in the (101) crystallographic plane.

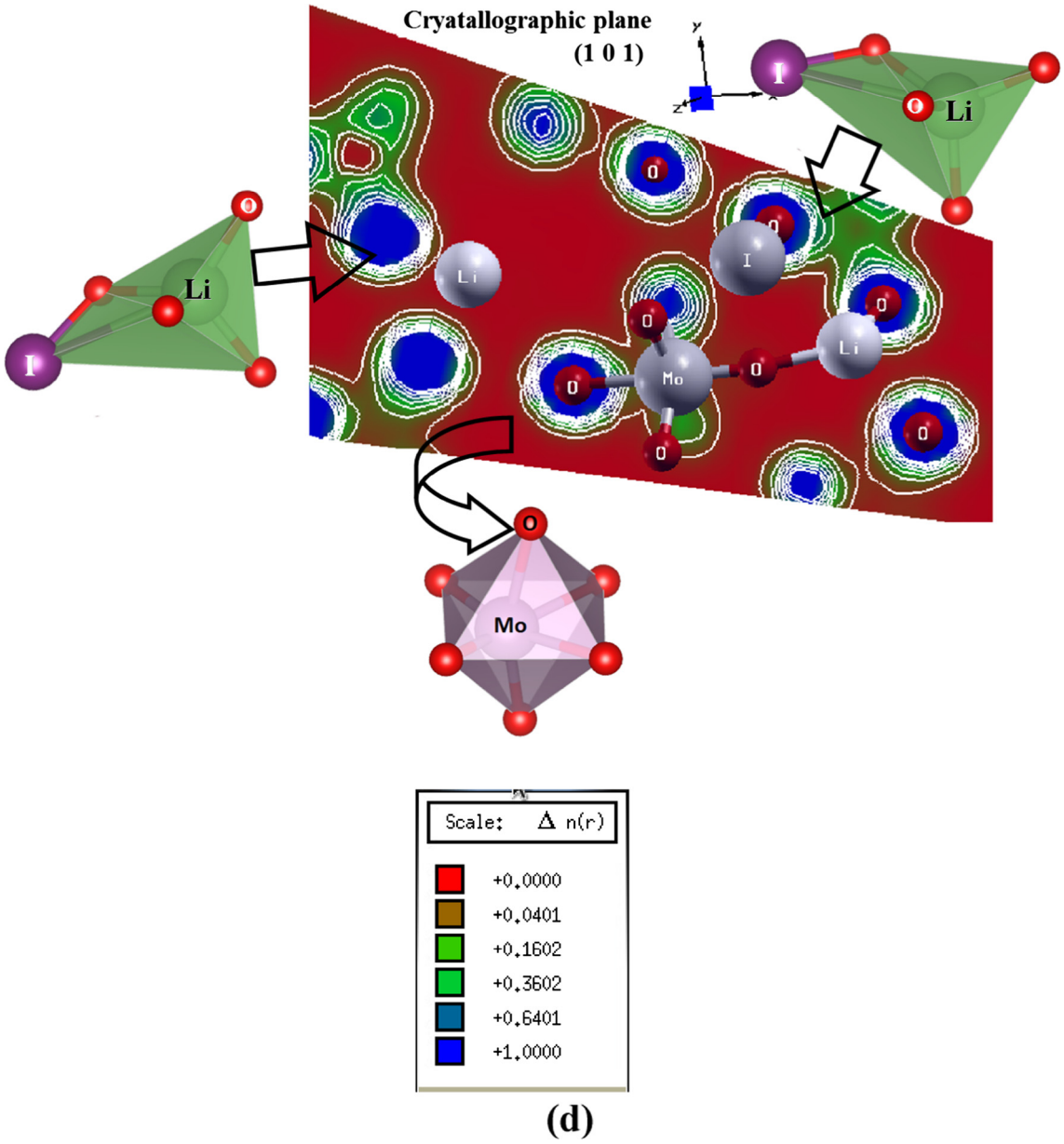

Fig. 4 (*continued*)

Table 2
Calculated bond lengths obtained by PBE-GGA in comparison with the experimental data [12].

Bond	Exp.	This work	Bond	Exp.	This work
Mo—O6	1.727(6)	1.733	I—O5	1.791(7)	1.751
Mo—O1	1.778(6)	1.788	I—O2	1.820(6)	1.857
Mo—O3	1.780(6)	1.799	Li—O4	1.95(2)	1.929
Mo—O1	2.135(6)	2.121	Li—O4	1.96(2)	1.929
Mo—O3	2.145(6)	2.137	Li—O6	1.97(2)	1.961
Mo—O2	2.163(6)	2.157	Li—O5	2.10(2)	2.091
I—O4	1.791(7)	1.820			

Table 3
Calculated bond angles obtained by PBE-GGA in comparison with the experimental data [12].

Bond angle	Exp. (°)	This work (°)	Bond angle	Exp. (°)	This work (°)
O6—Mo—O1	102.4(3)	102.50	O1—Mo—O3	76.8(3)	76.76
O6—Mo—O3	102.3(3)	101.90	O6—Mo—O2	163.3(3)	163.23
O1—Mo—O3	101.5(3)	101.39	O1—Mo—O2	87.9(3)	87.79
O6—Mo—O1	90.6(3)	90.31	O3—Mo—O2	88.2(3)	88.0
O1—Mo—O1	89.31(9)	89.29	O1—Mo—O2	76.3(3)	76.40
O3—Mo—O1	160.9(3)	160.69	O3—Mo—O2	76.5(2)	76.47
O6—Mo—O3	90.6(3)	90.71	O3—Mo—O2	100.6(3)	100.4
O1—Mo—O3	161.1(3)	159.99	O4—I—O2	98.3(3)	98.2
O3—Mo—O3	88.85(8)	88.81	O5—I—O2	96.3(3)	96.4

obtained results show that the novel molybdenyl iodate $LiMoO_3$ (IO_3) is an active photocatalyst under visible light irradiation.

Acknowledgments

The results were developed within the CENTEM project, Reg. No. CZ.1.05/2.1.00/03.0088, cofunded by the ERDF as part of the Ministry of Education, Youth and Sports OP RDI program and, in the follow-up sustainability stage, supported through CENTEM PLUS (LO1402) by financial means from the Ministry of Education, Youth and Sports under the "National Sustainability Programme I." Computational resources were provided by MetaCentrum (LM2010005) and CERIT-SC (CZ.1.05/3.2.00/08.0144) infrastructures. SA would like to thank CSIR-NPL and the Physics Department IIT Delhi for financial support.

References

[1] X. Chen, C. Li, M. Gratzel, R. Kostecki, S.S. Mao, Chem. Soc. Rev. 41 (2012) 7909–7937.
[2] Q. Zhang, C.S. Dandeneau, X. Zhou, G. Cao, Adv. Mater. 21 (2009) 4087–4108.
[3] S.K. Cushing, J. Li, F. Meng, T.R. Senty, S. Suri, M. Zhi, M. Li, A.D. Bristow, N. Wu, J. Am. Chem. Soc. 134 (2012) 15033–15041.
[4] H. Wang, X. Yuan, Y. Wu, H. Huang, X. Peng, G. Zeng, H. Zhong, J. Liang, M. Ren, Adv. Colloid Interface Sci. 195–196 (2013) 19–40.
[5] J. Di, J. Xia, M. Ji, B. Wang, S. Yin, H. Xu, Z. Chen, H. Li, Langmuir 32 (2016) 2075–2084.
[6] L. Zhang, W. Wang, S. Sun, D. Jiang, Appl. Catal. B Environ. 168–169 (2015) 9–13.
[7] H. Wang, X. Yuan, G. Zeng, Y. Wu, Y. Liu, Q. Jiang, S. Gu, Adv. Colloid Interface Sci. 221 (2015) 41–59.
[8] S. Bai, J. Jiang, Q. Zhang, Y.J. Xiong, Chem. Soc. Rev. 44 (2015) 2893–2939.
[9] A.L. Linsebigler, G.Q. Lu, J.T. Yates, Chem. Rev. 95 (1995) 735–758.
[10] J. Schneider, M. Matsuoka, M. Takeuchi, J.L. Zhang, Y. Horiuchi, M. Anpo, D.W. Bahnemann, Chem. Rev. 114 (2014) 9919–9986.
[11] S. Bai, X.Y. Li, Q. Kong, R. Long, C.M. Wang, J. Jiang, Y.J. Xiong, Adv. Mater. 27 (2015) 3444–3452.
[12] X. Chen, L. Zhang, X. Chang, H. Xue, H. Zang, W. Xiao, X. Song, H. Yan, J. Alloys Compd. 428 (2007) 54–58.
[13] R.E. Sykora, K.M. Ok, P.S. Halasyamani, J. Am. Chem. Soc. 124 (2002) 1951–1957.
[14] R.E. Sykora, D.M. Wells, T.E. Albrecht-Schmitt, J. Solid State Chem. 166 (2002) 442–448.
[15] H.S. Ra, K.M. Ok, P.S. Halasyamani, J. Am. Chem. Soc. 125 (2003) 7764–7765.
[16] E.O. Chi, E.K.M. Ok, Y. Porter, P.S. Halasyamani, Chem. Mater. 18 (2006) 2070–2074.
[17] B.P. Yang, C.L. Hu, X. Xu, C.F. Sun, J.H. Zhang, J.G. Mao, Chem. Mater. 22 (2010) 1545–1550.
[18] C.F. Sun, C.L. Hu, X. Xu, L.B. Ling, T. Hu, F. Kong, X.F. Long, J.G. Mao, J. Am. Chem. Soc. 131 (2009) 9486–9487.
[19] C.L. Hu, J.G. Mao, J. Phys. Condens. Matter 22 (2010) 155801.
[20] L. Sandhya Kumari, P. Prabhakar Rao, S. Sameera, V. James, Mater. Res. Bull. 70 (2015) 93–98.
[21] J. Feng, H. Huang, S. Yu, F. Dong, Y. Zhang, Phys. Chem. Chem. Phys. 18 (2016) 7851–7859.
[22] S. Yu, H. Huang, F. Dong, M. Li, N. Tian, T. Zhang, Y. Zhang, A.C.S. Appl, Mater. Interfaces 7 (2015) 27925–27933.
[23] Y. Huang, H. Li, W. Fan, F. Zhao, W. Qiu, H.-B. Ji, Y. Tong, A.C.S. Appl, Mater. Interfaces 8 (2016) 27859–27867.
[24] H. Huang, K. Xiao, K. Liu, S. Yu, Y. Zhang, Cryst. Growth Des. 16 (2016) 221–228.
[25] H. Huang, Y. He, R. He, X. Jiang, Z. Lin, Y. Zhang, S. Wang, Inorg. Chem. Commun. 40 (2014) 215–219.
[26] P.S. Halasyamani, Chem. Mater. 16 (2004) 3586–3592.
[27] R.G. Pearson, J. Am. Chem. Soc. 91 (1969) 4947–4955.
[28] R.A. Wheeler, M.H. Whangbo, T. Hughbanks, R. Hoffmann, J.K. Burdett, T.A. Albright, J. Am. Chem. Soc. 108 (1986) 2222–2236.
[29] M.I. Kolinko, I.V. Kityk, A.S. Krochuk, J. Phys. Chem. Solids 53 (1992) 1315–1320.
[30] A. Majchrowski, J. Ebothe, E. Gondek, K. Ozga, I.V. Kityk, A.H. Reshak, T. Łukasiewicz, J. Alloys Compd. 485 (485) (2009) 29–32.
[31] J.P. Perdew, S. Burke, M. Ernzerhof, Phys. Rev. Lett. 77 (1996) 3865.
[32] F. Tran, P. Blaha, Phys. Rev. Lett. 102 (2009) 226401.
[33] A.H. Reshak, RSC Adv. 5 (2015) 22044.
[34] A.H. Reshak, H. Huang, H. Kamarudin, S. Auluck, J. Appl. Phys. 117 (2015) 085703.
[35] A.H. Reshak, RSC Adv. 5 (2015) 33632–33638.
[36] L. Ma, Z. Xia, V. Atuchin, M. Molokeev, S. Auluck, A.H. Reshak, Q. Liu, Phys. Chem. Chem. Phys. 17 (2015) 31188–31194.
[37] F.S. Sergey, V.V. Atuchin, Z.A. Solodovnikova, O.Y. Khyzhun, M.I. Danylenko, D. P. Pishchur, P.E. Plyusnin, A.M. Pugachev, T.A. Gavrilova, A.P. Yelisseyev, A.H. Reshak, Z.A. Alahmed, N.F. Habubi, Inorg. Chem. 56 (2017) 3276–3286.
[38] G.E. Davydyuk, O.Y. Khyzhun, A.H. Reshak, H. Kamarudin, G.L. Myronchuk, S.P. Danylchuk, A.O. Fedorchuk, L.V. Piskach, M.Yu. Mozolyuk, O.V. Parasyuk, Phys. Chem. Chem. Phys. 15 (2013) 6965.
[39] A.H. Reshak, Phys. Chem. Chem. Phys. 16 (2014) 10558.
[40] A.H. Reshak, Y.M. Kogut, A.O. Fedorchuk, O.V. Zamuruyeva, G.L. Myronchuk, O. V. Parasyuk, H. Kamarudin, S. Auluck, K.L. Plucinskig, J. Bila, Phys. Chem. Chem. Phys. 15 (2013) 18979.
[41] A.H. Reshak, D. Stys, S. Auluck, I.V. Kityk, Phys. Chem. Chem. Phys. 13 (2011) 2945.
[42] H. Huang, Y. He, X. Li, M. Li, C. Zeng, F. Dong, X. Du T. Zhang, Y. Zhang, J. Mater. Chem. A 3 (2015) 24547-24556.
[43] H. Huang, Y. He, Z. Lin, L. Kang, Y. Zhang, J. Phys. Chem. C 117 (2013) 22986–22994.
[44] J. Zhang, W. Yu, J. Liu, B. Liud, Appl. Surf. Sci. 358 (2015) 457–462.
[45] X. Li, J. Zhao, J. Yang, Sci. Rep. 3 (2013) 1858.
[46] P. Blaha, K. Schwarz, G. K. H. Madsen, D. Kvasnicka and J. Luitz, WIEN2k, An augmented plane wave plus local orbitals program for calculating crystal properties, Vienna University of Technology, Austria (2001).
[47] K. Schwarz, P. Blaha, Comput. Mater. Sci. 28 (2003) 259.
[48] P.E. Blöchl, O. Jepsen, O.K. Andersen, Phys. Rev. B Condens. Matter 49 (1994) 16223.